Nanoscale

Accepted Manuscript

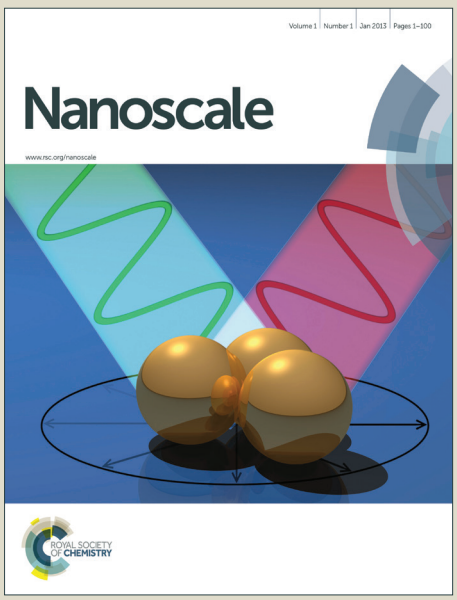

ROYAL SOCIETY OF CHEMISTRY

www.rsc.org/nanoscale

Cite this: DOI: 10.1039/c0xx00000x

www.rsc.org/xxxxxx

PAPER

Low-temperature solution-processable $Ni(OH)_2$ ultrathin nanosheet/N-graphene nanohybrids for high-performance supercapacitor electrodes†

Haixin Chang,[a,b]* Jianli Kang,[a,]* Luyang Chen,[a] Junqiang Wang,[a] Kazuyo Ohmura,[c] Na Chen,[a] Takeshi Fujita,[a] Hongkai Wu,[a,d,]* Mingwei Chen[a]

Received (in XXX, XXX) Xth XXXXXXXXX 20XX, Accepted Xth XXXXXXXXX 20XX
DOI: 10.1039/b000000x

A novel and facile strategy is developed to fabricate highly nitrogen-doped graphene (N-graphene) based nanohybrids with ultrathin nanosheet nanocrystals using a low-temperature, solution processing method for high-performance supercapacitor electrodes. High N doping can be achieved together with one of the lowest oxygenous contents in chemically-reduced graphene and related nanohybrids at low temperature inspired by the large scale residue defects of chemically-reduced graphene. The high-quality ultrathin $Ni(OH)_2$ nanosheet nanocrystal/N-graphene layered nanohybrids can be applied as supercapacitor electrodes with ultrahigh capacitances of ~1551 F/g, excellent rate performance in the scan rate from 2 to 100 mV/s and in the discharge current from 1.5 A/g to 30 A/g and good cycling stability. Moreover, the capacitance of $Ni(OH)_2$ nanosheet/N-graphene nanohybrids is two and one orders of magnitude higher than that for pure nanocrystals and that for the physical mixture of nanocrystal/N-graphene, respectively. Electron transfer in supercapacitor electrodes based on nanohybrids is over 100 times faster than that in electrodes from pure nanocrystals and several tens of times faster than that in electrodes from nanocrystal/N-graphene mixture. The results provide a low-cost, solution-processable and easily scalable route to high-performance graphene nanohybrid electrodes for energy applications.

1. Introduction

Graphene has great potential in various applications for its unique electronic properties.[1-5] Much attention has been paid to manipulate the electronic properties of graphene by size effect, defect, interface and hybrid.[5-15] Atomic doping can alter the electronic properties of graphene intrinsically and modify the local composition and electronic structure by including foreign atoms in matrix. Recently, nitrogen (N) doped graphene has attracted a lot of endeavors for its excellent performance in electronic devices.[16-25] There are usually three routes to achieve N doping in graphene, including doping during chemical vapor deposition (CVD) growth,[16] high temperature thermal annealing or decomposition with N containing species,[17] and NH_3/N_2 plasma.[18,19] These methods are not solution-processable and need high-temperature processing like thermal annealing/deposition or expensive equipments, limiting the cost and large scale applications. Despite many efforts, however, direct low-temperature, solution-processable N doping in graphene or reduced graphene is still a challenge.

Meanwhile, due to the low capacitance of commercial carbon-based electrical double layer capacitor, metal oxide-based Faradaic pseudocapacitive electrodes have been recognized as one of the most potential alternative supercapacitor electrodes.[26-36] Metal oxides usually have low conductivity and their hybrids with more conductive scaffolds are expected to improve the electron transfer in electrodes and capacitive performance. For example, nanoporous gold and carbon nanotubes (CNTs) are applied as conductive scaffolds for hybrid supercapacitor electrodes to improve the capacitive performance of metal oxides.[26,27,37-40] However, these kinds of scaffolds are expensive and low-cost high-quality scaffolds for metal oxide hybrids with efficient electron transfer in electrodes are highly expected. N-graphene, due to its improved electronic conductivity with N doping and two-dimensional structures, is a very potential alternative to nanoporous metal and CNTs in hybrid supercapacitor electrodes.

Chemically-reduced graphene from exfoliated graphite oxide is one of most available graphene and the only type of graphene to date which can be produced by the ton.[41] Here, inspired by the large scale residue defects in chemically-reduced graphene, a novel and facile method was developed to prepare solution-processable N-doped graphene (N-graphene) and related N-graphene nanohybrids with $Ni(OH)_2$ nanosheet nanocrystals at low-temperature based on chemically-reduced graphene. It was found for the first time that high N doping can be achieved even in chemically-reduced graphene by low temperature, solution-processed way due to the large scale residue defects. Moreover,

simultaneous *in situ* growth of $Ni(OH)_2$ nanosheet nanocrystals was achieved with a close contact with N-graphene by applying a negatively-charged surfactant as the growth medium and the resulted layered nanohybrids demonstrate an ultrahigh capacitance of ~1551 F/g for graphene hybrid electrodes with excellent rate performance (from 2 to 100 mV/s and from 1.5 A/g to 30 A/g) and good cycling stability. The N-graphene hybrid electrodes also show over 100 times higher electron transfer rate than pure nanocrystals and several times higher than nanocrystals/N-graphene mixture, leading to at least one order of magnitude higher capacitance in hybrid electrodes than other two types of electrodes. This low-temperature method may provide a novel route to large scale N-graphene nanohybrids for high performance electrodes in energy storage and conversion.

2. Results and discussion

The two-step method was developed for preparing highly N doped graphene at low temperature, starting from graphene oxide modified by negatively-charged surfactant (**Figure 1**). The surfactant-modified graphene oxide (S-graphene oxide) was first reduced by normal chemical method, e.g., using hydrazine in the presence of surfactant. Then obtained chemically-reduced graphene was further processed under 150 ºC with hydrothermal treatments in the presence of $NH_3 \cdot H_2O$. This strategy can be further used to prepare various N-doped graphene/nanosheet nanocrystal hybrids, where metal salt was added to the chemically-reduced graphene before hydrothermal reactions (**Figure 1**). Facile *in situ* nanocrystal growth on N-graphene achieved high-quality N-graphene based hybrid easily.

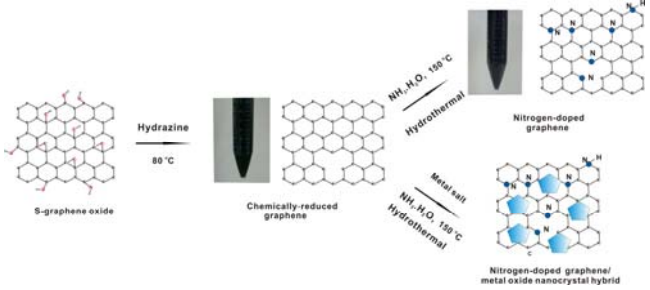

Figure 1. Scheme for low-temperature, solution-processable N doping in chemically-reduced graphene and nanosheet nanocrystal/N-graphene hybrids. S-graphene oxide: surfactant-modified graphene oxide. Solution concentration for chemically-reduced graphene and nitrogen-doped graphene (N-graphene): 1 mg/mL.

The obtained N-graphene is highly solution processable in aqueous solutions (e.g., 1 mg/mL, **Figure 1**). N-graphene had high quality with strong six-fold symmetry in the diffractions. The intensity of {1-210} diffractions were lower than {0-110} diffractions, indicating single layer sheet or random stacks of single layer sheets for the sample.[42] TEM images showed the N-graphene was very flexible with tiny wrinkles on the surfaces (**Figure 2**). Raman spectra were also applied to characterize the graphene oxide, chemically-reduced graphene and N-graphene. G peak of Raman spectra shifted from ~1602 cm^{-1} for graphene oxide to ~1589 cm^{-1} for chemically-reduced graphene (**Figure 3**).[5a,5b] The G peak for chemically-reduced graphene shifted slightly to ~1592 cm^{-1} for N-graphene (**Figure 3**). The ratio of I_D/I_G is even larger in chemically-reduced graphene than that in graphene oxide, indicating a large scale of residue defects after chemical reduction. The large scale residue defects enhanced the feasibility of direct doping nitrogen to chemically-reduced graphene even at low temperature.

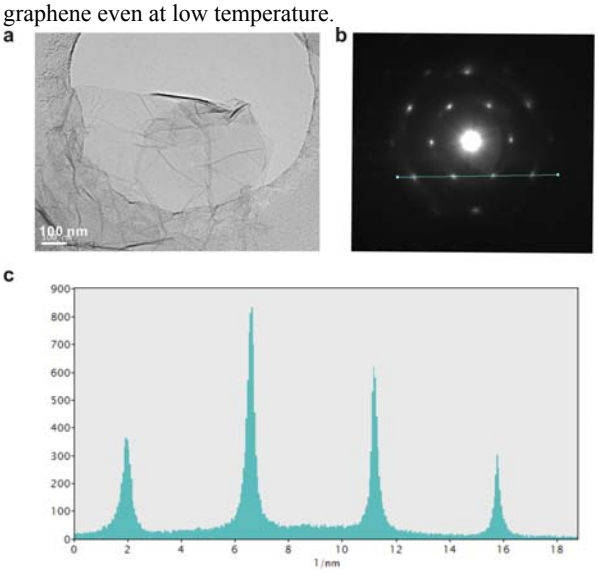

Figure 2. TEM image and diffraction for N-graphene. (a) TEM image. (b) Electron diffraction pattern. c, Intensity profile of the cross line in b.

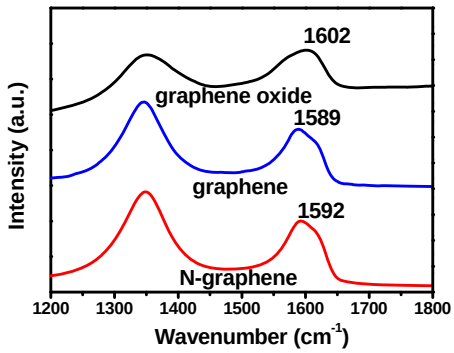

Figure 3. Raman characterizations of graphene oxide, graphene and N-graphene.

X-ray photoelectron spectra (XPS) measurements were then conducted to study the atomic species and chemical bonds in the N-graphene (**Figure 4**). Obvious N doping was observed in N doped graphene with N/C ratio of up to ~4.5% (**Figure 4a**). The N doping in graphene usually has several type of N dopants. The peak-fitting analysis of N 1s XPS spectra indicated that there were three fitting peaks in N 1s spectra and was consistent with previous studies (**Figure 4b**).[18] N dopants include pyridinic N (~398.7 eV), pyrrolic N (~399.7 eV) and graphitic N (~401.4 eV) types with percentage of ~6.9%, 27.2% and 65.9%, respectively. The large part of graphitic N doping is induced by the large scale residue defects in the chemically-reduced graphene. Analysis of C 1s XPS spectra also showed the significant decrease of oxygenous groups both in chemically-reduced graphene and N

doped graphene (**Figure 4c**), comparing with that in graphene oxide. The O/C atomic ratio decreased from ~50% in graphene oxide to 12% in chemically-reduced graphene, and to as low as ~7% in N-graphene. The present N-graphene has one of the lowest oxygenous contents in low-temperature processed chemically-reduced graphene, which are normally achieved only in ultrahigh temperature processing under inert protected gas. Importantly, the N doping in graphene is stable in the solution and no obvious lose of N doping is observed even after over 6 months storage. These excellent chemical characteristics in two-step N-graphene are expected to improve the electronic transport in N-graphene by removing most oxygenous electron scattering and trapping centers.

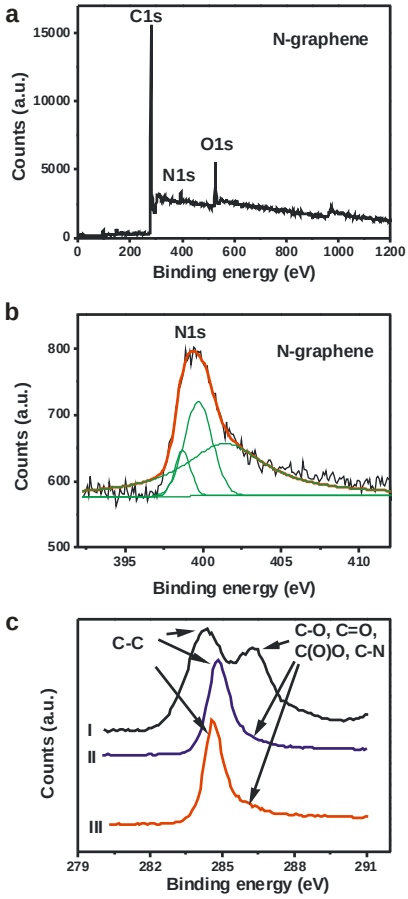

Figure 4. XPS characterizations of N-graphene. (a) Survey scan of N-graphene. (b) Detail scan and multi-peak fitting of N 1s in N-graphene, (c) Comparison of C1s spectra of graphene oxide (I), graphene (II), and N-graphene (III).

The strategy can be further modified to prepare metal hydroxide ultrathin nanosheet nanocrystal/N-graphene hybrids for high performance supercapacitor electrodes. By introducing metal salt with $NH_3 \cdot H_2O$ in the chemically-reduced graphene, metal hydroxide ultrathin nanosheet nanocrystal/N-graphene layered nanohybrids or heterostructures can be simultaneously achieved during the transformation of chemically-reduced graphene to N-graphene (**Figure 1**). As a demonstration, $Ni(OH)_2$/N-graphene nanohybrids were developed using this strategy. X-ray diffraction (XRD) results showed the nickel hydroxide nanocrystals were successfully included in the hybrid with N-graphene (**Figure 5a**). The XRD patterns are analyzed and applied to identify the resulted nickel compounds. The peaks at ~18º and ~39º indicate (001) and (002) diffraction planes of β phase $Ni(OH)_2$, respectively, while the peaks at ~12º and ~21º indicate the (003) and (006) diffraction planes of α phase $Ni(OH)_2$, consistent with previous reports on $Ni(OH)_2$.[32,43] The XRD patterns in $Ni(OH)_2$ and $Ni(OH)_2$/N-graphene nanohybrids imply the resulted $Ni(OH)_2$ nanocrystals were a mixture of α and β phases. XPS spectra further confirm the existences of N doping in $Ni(OH)_2$/N-graphene nanohybrids with a N/C ratio of ~4% (**Figure 5b**). Usually the weight ratio of $Ni(OH)_2$ nanocrystals in the $Ni(OH)_2$/N-graphene hybrids was ~70%.

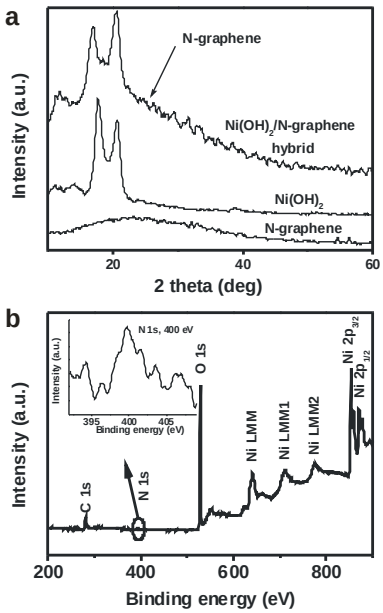

Figure 5. XRD and XPS characterization of $Ni(OH)_2$/N-graphene hybrid. (a) XRD spectra of N-graphene, $Ni(OH)_2$, and $Ni(OH)_2$/N-graphene hybrid. (b) XPS spectra of $Ni(OH)_2$/N-graphene hybrid. Inset in b, N 1s spectra of the hybrid.

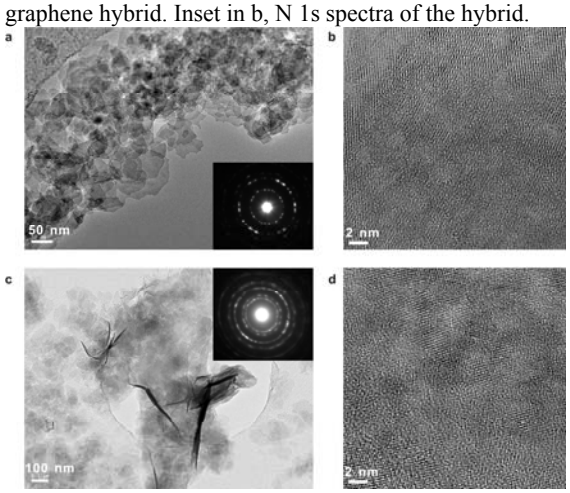

Figure 6. TEM images of $Ni(OH)_2$ nanosheet nanocrystals (a, b) and $Ni(OH)_2$/N-graphene hybrid (c, d). Inset in a and c, electron diffraction patterns of $Ni(OH)_2$ nanocrystal (a) and $Ni(OH)_2$/N-graphene hybrid (c).

The morphologies of $Ni(OH)_2$ ultrathin nanosheet nanocrystals and $Ni(OH)_2$/N-graphene nanohybrids were further studied by transmission electron microscopy (TEM) (**Figure 6**). Ultrathin $Ni(OH)_2$ nanocrystals were usually formed with a size from a

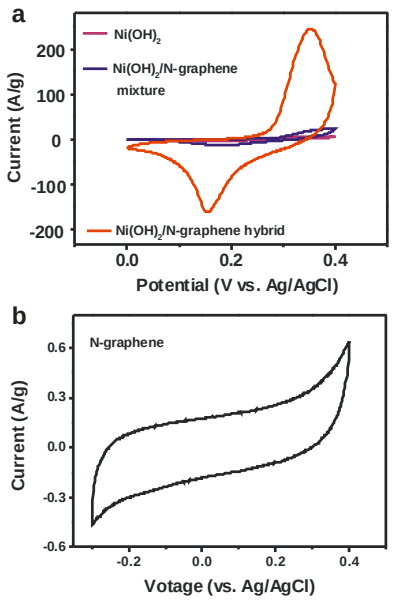

Figure 7. (a) Cyclic voltammetry curves of electrodes based on $Ni(OH)_2$, $Ni(OH)_2$/N-graphene mixture and $Ni(OH)_2$/N-graphene hybrid. (b) Cyclic voltammetry curve of electrodes based on N-graphene. Scan rates: 50 mV/s.

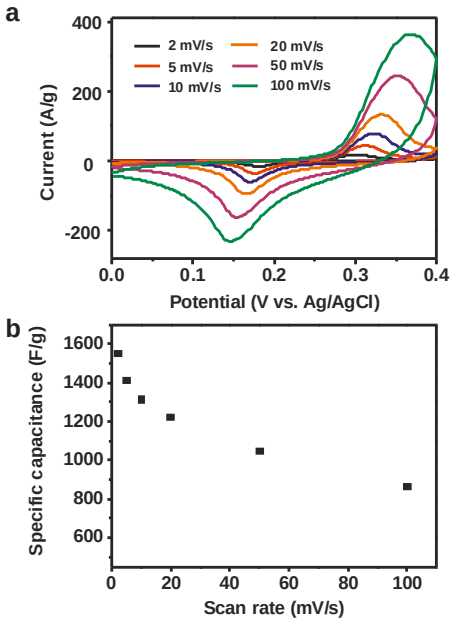

Figure 8. Electrochemical capacitive performance of $Ni(OH)_2$/N-graphene hybrid electrodes from cyclic voltammetry measurements. (a) Cyclic voltammetry curves at different scan rates. (b) Calculated specific capacitances at different scan rates.

few tens to a few hundreds nanometers with a thickness of a few nanometers (**Figure 6a and 6b**). In the presence of N-graphene, ultrathin $Ni(OH)_2$ nanocrystals were grown in situ on N-graphene and formed close contacts with N-graphene whose surfaces were mostly covered by $Ni(OH)_2$ nanosheet nanocrystals (**Figure 6c and 6d**). High-resolution TEM images demonstrate no obvious differences in atomic structure for pure $Ni(OH)_2$ nanocrystals and $Ni(OH)_2$ nanocrystals in $Ni(OH)_2$/N-graphene hybrids (**Figure 6b and 6d**), which is consistent with the XRD spectra (**Figure 5a**). The in situ growth of $Ni(OH)_2$ nanocrystal on N-graphene was further confirmed by the electron diffractions in pure $Ni(OH)_2$ and $Ni(OH)_2$/N-graphene hybrids (Inset in **Figure 6a and 6c**). Most importantly, this close contact will help the electronic transfer between nanosheet nanocrystals and N-graphene when forming supercapacitor electrodes. No G peak shift in Raman spectra was observed (**Figure S1**), implying no obvious damages of N-graphene were induced by the *in situ* growth and close contacts of $Ni(OH)_2$ nanocrystals.

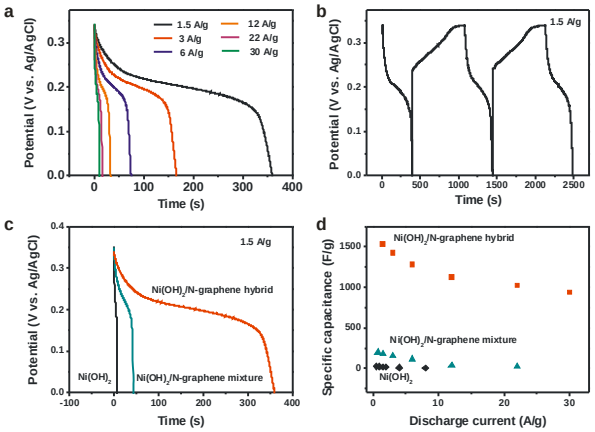

Figure 9. Electrochemical capacitive performance of $Ni(OH)_2$/N-graphene hybrid electrodes from discharge measurements. (a) Discharge curves at different discharge current of $Ni(OH)_2$/N-graphene hybrid electrodes. (b) Three discharge cycles for $Ni(OH)_2$/N-graphene hybrid electrodes at discharge current of 1.5 A/g. (c) Calculated specific capacitance for electrodes based on $Ni(OH)_2$/N-graphene hybrid, pure $Ni(OH)_2$ nanocrystals, and $Ni(OH)_2$/N-graphene mixture at discharge current of 1.5 A/g. (d) Capacitance comparison of electrodes based on $Ni(OH)_2$/N-graphene hybrid, pure $Ni(OH)_2$, and $Ni(OH)_2$/N-graphene mixture at different discharge currents.

The electrochemical performance of $Ni(OH)_2$/N-graphene hybrid electrodes were measured using cyclovometry (CV) and charge-discharge techniques. The CV measurements show $Ni(OH)_2$/N-graphene hybrids have a much higher current density than pure $Ni(OH)_2$ nanocrystals and $Ni(OH)_2$/N-graphene mixtures with the same amount of $Ni(OH)_2$ (**Figure 7a**). The current density of electrodes based on pure N-graphene is two magnitudes of order lower than $Ni(OH)_2$/N-graphene hybrids with neglectable capacitance (**Figure 7b**). The comparisons indicate the N-graphene play a very significant role in the hybrid electrodes. Importantly, the $Ni(OH)_2$/N-graphene hybrid electrodes showed an over one order of magnitude higher current density than that in $Ni(OH)_2$/N-graphene mixture, implying that the close contact and connection between N-graphene and $Ni(OH)_2$ nanosheet nanocrystals induced by *in situ* growth mediated by negatively-charged surfactant were very important

for the performance of the hybrid electrodes. The specific capacitance of the hybrid supercapacitor electrodes can reach as high as ~1551 F/g at 2 mV/s (based on the mass of $Ni(OH)_2$, ~1086 F/g based on the mass of $Ni(OH)_2$/N-graphene hybrids), and ~1413 F/g at 5 mV/s. Even at a high san rate of 50 mV/s, the specific capacitance keeps at ~1046 F/g, ~70% of the original capacitance (**Figure 8**). Further increasing the scan rate up to 100 mV/s, the capacitance is still over 60% of the original capacitance. The control measurements of pure glassy carbon electrodes demonstrate a neglectable tiny electrochemical current and capacitance (**Figure S2**). The galvanostatic charge-discharge measurements show a similar trend with the capacitance of ~1536 F/g at 1.5 A/g (based on the mass of $Ni(OH)_2$, ~1075 F/g based on the mass of $Ni(OH)_2$/N-graphene hybrids), ~1424 F/g at 3 A/g, and 1125 F/g at 12 A/g, and kept over 60% of original capacitance even at 30 A/g (**Figure 9**). Moreover, the specific capacitance of the $Ni(OH)_2$/N-graphene hybrid electrodes is over 7 times higher than that in $Ni(OH)_2$/N-graphene mixture and over 60 times higher than that in pure $Ni(OH)_2$ nanocrystals (**Figure 9b and 9c**). The capacitance of the N-graphene/nanocrystal hybrid supercapacitor electrodes is higher than that of hybrid electrodes based on chemically-reduced graphene (~1267 F/g at 5 mV/s)[32] and CVD-grown graphene foam (816 F/g at 5 mV/s).[33] More importantly, the $Ni(OH)_2$/N-graphene hybrid supercapacitor electrodes have excellent rate performance with ~70% of the original capacitance at a discharge current of 22 A/g while only ~14% at 22 A/g for $Ni(OH)_2$/N-graphene mixture and ~25% at 8 A/g for pure $Ni(OH)_2$ nanocrystals are observed (**Figure 9d**). The $Ni(OH)_2$/N-graphene hybrid supercapacitor electrodes also demonstrate good performance in cycling stability. The capacitance for electrodes increases progressively due to activation process in the beginning,[26c] and has no obvious degradation for 2500 cycles (**Figure 10**).

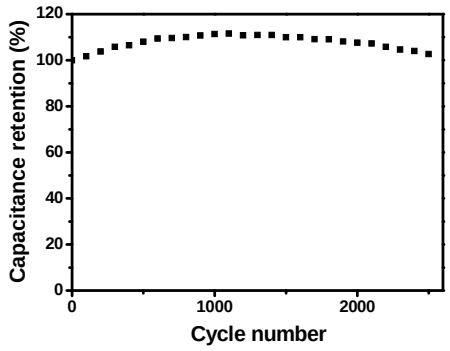

Figure 10. Cycling electrochemical stability for $Ni(OH)_2$/N-graphene hybrid electrodes.

The ultrahigh capacitance and excellent rate performance and good cycling stability are partially attributed to the high quality of N-graphene and smooth electron transfer between in situ grown nanosheet nanocrystals and N-graphene. The electron transfer properties in the $Ni(OH)_2$/N-graphene hybrid electrodes were investigated by the electrochemical impedance spectra (**Figure 11**). The $Ni(OH)_2$/N-graphene hybrid has much smaller electron transfer resistance than that in pure $Ni(OH)_2$ nanocrystals and $Ni(OH)_2$/N-graphene mixture (**Figure 11**). The electron transfer resistance (R_{et}) is less than 200 ohm for $Ni(OH)_2$/N-graphene hybrids while at the level of ~15000 ohm for $Ni(OH)_2$/N-graphene mixtures and at the level of ~80000 ohm for pure $Ni(OH)_2$ nanocrystals. In general, electron transfer in $Ni(OH)_2$/N-graphene hybrid electrodes is over 100 times faster than that in pure $Ni(OH)_2$ nanocrystals, and several tens of times faster than that in $Ni(OH)_2$/N-graphene mixture. The smooth electron transfer between nanosheet nanocrystals and N-graphene will improve the capacitance, high rate performance and stability in the electrodes as mentioned above. All these electrochemical measurements indicated that the solution-processable N-graphene nanohybrids could be an excellent platform for applications in supercapacitor electrodes, considering its low cost because of wet chemical synthesis and solution processability of N-graphene.

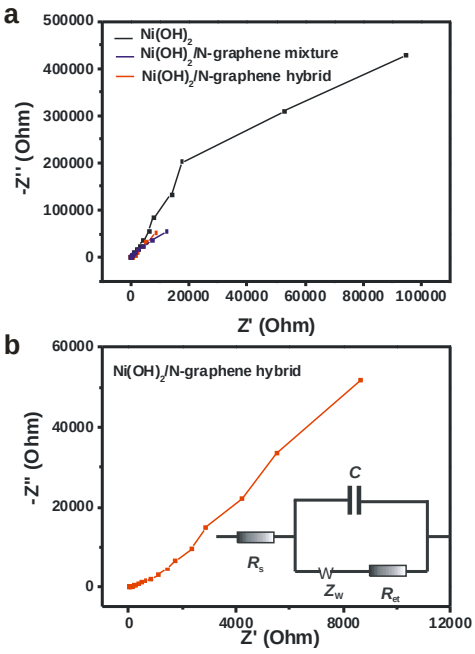

Figure 11. Electrochemical impedance spectra of $Ni(OH)_2$, $Ni(OH)_2$/N-graphene mixture and $Ni(OH)_2$/N-graphene hybrid electrodes. (a) Electrochemical impedance spectra of three electrodes. (b) Enlarge view of electrochemical impedance spectra of $Ni(OH)_2$/N-graphene hybrid electrode. Inset in b, analytical model for impedance spectra where Rs is resistance of electrolyte, Ret electron transfer resistance, C capacitance and Zw Warburg impedance. Frequency: 100 kHz-0.1 Hz.

3. Conclusion

A novel and facile two-step strategy was developed for preparing solution-processable, N-doped graphene and related layered nanohybrids with *in situ* grown $Ni(OH)_2$ ultrathin nanosheet nanocrystals at low temperature for supercapacitor electrodes. The obtained N-graphene has high N doping and lowest oxygenous content by low-temperature processing methods. N-graphene nanohybrids with $Ni(OH)_2$ nanosheet nanocrystals demonstrate ultrahigh capacitances of ~1551 F/g, excellent rate performance from 2 to 100 mV/s and from 1.5 A/g to 30 A/g and good cycling stability. The high electrochemical performance of N-graphene hybrid electrodes results from the unique electronic properties of N–graphene and ultrahigh enhancement of electron transfer between ultrathin nanosheet

nanocrystals and N-graphene in the hybrid electrodes. The strategy is also compatible with other various nanocrystals such as transition metal and metal dichalcogenides nanocrystals. Thereby the low temperature, solution-processable, high quality N-graphene and related nanohybrids may facilitate the large scale applications of N-graphene hybrids in energy storage and conversion.

4. Experimental

Fabrication of N-graphene and $Ni(OH)_2$ nanosheet/N-graphene nanohybrids:

Graphite oxide was fabricated following the previous reports.[5] The graphite oxide was dissolved in deionized (DI) water and exfoliated in the presence of sodium dodecyl benzene sulfonate (SDBS) using ultrasonic processing. The resulted S-graphene oxide was firstly chemically reduced by hydrazine at 80 ºC under continuous stirring to achieve high quality chemically-reduced graphene. To prepare N-graphene, 1 mg/mL chemically-reduced graphene was dispersed in DI water then mixed with ammonia by a certain mixing weight ratio (ammonia/graphene=18) and transferred to a high pressure autoclave to keep the hydrothermal reactions at 150 ºC for 3 hours. The obtained N-graphene was washed by deionized water and ethanol thoroughly. To prepare the $Ni(OH)_2$ nanosheet/N-graphene nanohybrids, 1 mg/mL chemically-reduced graphene was first mixed with nickel salt ($Ni(NO_3)_2$ or $Ni(Ac)_2$) for 30 min and then mixed with ammonia with a certain ratio (1 mg graphene for 18 mg ammonia and 0.034 mmol nickel salts) in DI water under continuous stirring. The resulted mixture was transferred to a high pressure autoclave for hydrothermal reactions at 150 ºC for 3 hours. The mass of graphene before the $Ni(OH)_2$ nanocrystal growth and graphene nanohybrids after nanocrystal were measured by a high-sensitivity electronic balance (0.01 mg sensitivity, Mettler Toledo, Model AB135-S) to determine the loading amount of nanocrystals. The weight ratio of $Ni(OH)_2$ nanocrystals in $Ni(OH)_2$ nanosheet/N-graphene nanohybrids was ~70 wt.%. As a control, nickel salts and ammonia were mixed in the same ratio but without chemically-reduced graphene to prepare pure $Ni(OH)_2$ nanocrystals.

Characterizations and electrochemical measurements:

The TEM imaging was conducted by JEOL JEM-2010F transmission electron microscope with 200 kV accelerated voltage. The XPS spectra were collected from AXIS ultra DLD (Shimadzu Kratos) with a X-ray source of monochromatic Al-Kαunder 15kV and 10mA. XRD measurements were done by a Bruker D8 Advance diffractometer with a Cu-Kα radiation source. Raman spectra were measured from Laser Raman Microscope Raman-11 with a 540 nm laser (Nanophoton Co., Japan). To prepare electrodes for electrochemical measurements, $Ni(OH)_2$/N-graphene hybrids, pure $Ni(OH)_2$ nanocrystals or $Ni(OH)_2$/N-graphene mixture was mixed with Nafion (Sigma-Aldrich, 5% solution in a mixture of water and lower aliphatic alcohols-IPA) followed by drop-drying on freshly polished glassy carbon. The CV and charge-discharge measurements were done in 30 wt.% KOH solution by an electrochemical station (Ivium Technologies) using Ag/AgCl as reference electrode and Pt wire as counter electrode. The $Ni(OH)_2$/N-graphene hybrid electrodes were stabilized and activated by a number of electrochemical scan cycles before the measurements. The specific capacitance (C) is calculated by C = S/(2VUm) in CV measurements where S is area of CV curves, V scan rate, U potential window and m weight of $Ni(OH)_2$ in electrodes, or by C = I/(-dU/dt)m in discharge measurements where I is discharge current density, U potential window and t discharge time.[31,32] Electrochemical impedance spectra were collected by the same electrochemical station with a frequency from 100 kHz to 0.1 Hz.

Acknowledgements

This work was supported by World Premier International Research Center Initiative (WPI), MEXT, Japan. H.X.C. acknowledges the fundings from HUST, WPI-AIMR fusion research funding from MEXT and Grant-in-Aid for Young Scientists from JSPS (KAKENHI, No. 25870057), Japan. We also thank Advanced Research Center of Metallic Glasses in Institute for Materials Research (IMR), Tohoku University for XPS measurements.

‡ Notes and references

Authors Address

[a] *WPI-Advanced Institute for Materials Research, Tohoku University, Sendai 980-8577, Japan; E-mail: hxchang@wpi-aimr.tohoku.ac.jp (H.X.C.), jlkangnpm@126.com (J.K.)*

[b] *State Key Laboratory of Material Processing and Die & Mould Technology, School of Materials Science and Engineering, Huazhong University of Science and Technology (HUST), Wuhan 430074, China*

[c] *Institute for Materials Research, Tohoku University, Sendai 980-8578, Japan*

[d] *Department of Chemistry, The Hong Kong University of Science and Technology, Clear water Bay, Hong Kong; chhkwu@ust.hk (H.W.)*

† Electronic Supplementary Information (ESI) available: Figure S1 and S2 as noted in text. See DOI: 10.1039/b000000x/

References

1 A. K. Geim and K. S. Novoselov, *Nat. Mater.* 2007, **6**, 183.
2 Y. Zhu, S. Murali, W. Cai, X. Li, J. W. Suk, J. R. Potts and R. S. Ruoff, *Adv. Mater.* 2010, **22**, 3906.
3 M. J. Allen, V. C. Tung and R. B. Kaner, *Chem. Rev.* 2009, **110**, 132.
4 C. N. R. Rao, A. K. Sood, K. S. Subrahmanyam and A. Govindaraj, *Angew. Chem. Int. Ed.* 2009, **48**, 7752.
5 (a) H. X. Chang, Z. H. Sun, Q. H. Yuan, F. Ding, X. M. Tao, F. Yan and Z. J. Zheng, *Adv. Mater.* 2010, **22**, 4872. (b) H. X. Chang, G. F. Wang, A. Yang, X. M. Tao, X. Q. Liu, Y. D. Shen and Z. J. Zheng, *Adv. Funct. Mater.* 2010, **20**, 2893. (c) H. X. Chang and H. Wu, *Energy Environ. Sci.* 2013, **6**, 3483. (d) H. X. Chang and H. Wu, *Adv. Funct. Mater.* 2013, **23**, 1984. (e) H. X. Chang, Z. Sun, M. Saito, Q. Yuan, H. Zhang, J. Li, Z. Wang, T. Fujita, F. Ding, Z. Zheng, F. Yan, H. Wu, M. W. Chen and Y. Ikuhara, *Acs Nano* 2013, **7**, 6310. (f) J. Xia, F. Chen, J. H. Li and N. Tao, *Nat. Nanotechnol.* 2009, **4**, 505. (g) H. X. Chang, L. Tang, Y. Wang, J. H. Jiang and J. H. Li, *Anal. Chem.* 2010, **82**, 2341. (h) H. X. Chang, Z. Sun, K. Y.-F. Ho, X. Tao, F. Yan, W.-M. Kwok, Z. Zheng, *Nanoscale* 2011, **3**, 258.
6 X. L. Li, X. R. Wang, L. Zhang, S. W. Lee and H. J. Dai, *Science* 2008, **319**, 1229.
7 D. V. Kosynkin, A. L. Higginbotham, A. Sinitskii, J. R. Lomeda, A. Dimiev, B. K. Price and J. M. Tour, *Nature* 2009, **458**, 872.
8 K. P. Loh, Q. Bao, G. Eda and M. Chhowalla, *Nat. Chem.* 2010, **2**, 1015.
9 X. Dong, Y. Shi, W. Huang, P. Chen and L. J. Li, *Adv. Mater.* 2010, **22**, 1649.
10 Z. Chen, W. Ren, L. Gao, B. Liu, S. Pei and H.-M. Cheng, *Nat. Mater.* 2011, **10**, 424.

11 H. A. Becerril, J. Mao, Z. Liu, R. M. Stoltenberg, Z. Bao and Y. Chen, *Acs Nano* 2008, **2**, 463.

12 Q. Yu, L. A. Jauregui, W. Wu, R. Colby, J. Tian, Z. Su, H. Cao, Z. Liu, D. Pandey, D. Wei, T. F. Chung, P. Peng, N. P. Guisinger, E. A. Stach, J. Bao, S.-S. Pei and Y. P. Chen, *Nat. Mater.* 2011, **10**, 443.

13 J. Xu, K. Wang, S.-Z. Zu, B.-H. Han and Z. Wei, *Acs Nano* 2010, **4**, 5019.

14 X. Huang, Z. Yin, S. Wu, X. Qi, Q. He, Q. Zhang, Q. Yan, F. Boey and H. Zhang, *Small* 2011, **7**, 1876.

15 (a) P. Chen, T. Y. Xiao, Y. H. Qian, S. S. Li and S. H. Yu, *Adv. Mater.* 2013, **25**, 3192. (b) L. Peng, X. Peng, B. Liu, C. Wu, Y. Xie and G. Yu, *Nano Lett.* 2013, **13**, 2151.

16 (a) D. Wei, Y. Liu, Y. Wang, H. Zhang, L. Huang and G. Yu, Nano Lett. 2009, 9, 1752. (b) D. Usachov, O. Vilkov, A. Gruneis, D. Haberer, A. Fedorov, V. Adamchuk, A. Preobrajenski, P. Dudin, A. Barinov, M. Oehzelt, C. Laubschat and D. V. Vyalikh, *Nano Lett.* 2011, **11**, 5401.

17 (a) X. Li, H. Wang, J. T. Robinson, H. Sanchez, G. Diankov and H. Dai, *J. Am. Chem. Soc.* 2009, **131**, 15939. (b) X. Wang, X. Li, L. Zhang, Y. Yoon, P. K. Weber, H. Wang, J. Guo and H. Dai, *Science* 2009, **324**, 768.

18 Y.-C. Lin, C.-Y. Lin and P.-W. Chiu, *Appl. Phys. Lett.* 2010, **96**, 133110.

19 Y. Wang, Y. Shao, D. W. Matson, J. Li and Y. Lin, *Acs Nano* 2010, **4**, 1790.

20 L. Zhao, R. He, K. T. Rim, T. Schiros, K. S. Kim, H. Zhou, C. Gutiérrez, S. Chockalingam, C. J. Arguello and L. Pálová, *Science* 2011, **333**, 999.

21 Z.-S. Wu, S. Yang, Y. Sun, K. Parvez, X. Feng and K. Müllen, *J. Am. Chem. Soc.* 2012, **134**, 9082.

22 Z. Wen, X. Wang, S. Mao, Z. Bo, H. Kim, S. Cui, G. Lu, X. Feng and J. Chen, *Adv. Mater.* 2012, **24**, 5610.

23 X. Wang, X. Cao, L. Bourgeois, H. Guan, S. Chen, Y. Zhong, D. M. Tang, H. Li, T. Zhai and L. Li, *Adv. Funct. Mater.* 2012, **22**, 2682.

24 L. Qu, Y. Liu, J.-B. Baek and L. Dai, *Acs Nano* 2010, **4**, 1321.

25 B. Guo, Q. Liu, E. Chen, H. Zhu, L. Fang and J. R. Gong, *Nano Lett.* 2010, **10**, 4975.

26 (a) X. Lang, A. Hirata, T. Fujita and M. W. Chen, *Nat. Nanotechnol.* 2011, **6**, 232. (b) J. Kang, A. Hirata, L. Kang, X. Zhang, Y. Hou, L. Chen, C. Li, T. Fujita, K. Akagi and M. W. Chen, *Angew. Chem. Int. Ed.* 2013, **52**, 1664. (c) J. Kang, A. Hirata, H. J. Qiu, L. Chen, X. Ge, T. Fujita and M. W. Chen, *Adv. Mater.* 2014, **26**, 269. (d) J. Kang, L. Chen, Y. Hou, C. Li, T. Fujita, X. Lang, A. Hirata and M. W. Chen, *Adv. Energy Mater.* 2013, **3**, 857.

27 P. Simon and Y. Gogotsi, *Nat. Mater.* 2008, **7**, 845.

28 J. Jiang, Y. Li, J. Liu, X. Huang, C. Yuan and X. W. D. Lou, *Adv. Mater.* 2012, **24**, 5166.

29 W. Wei, X. Cui, W. Chen and D. G. Ivey, *Chem. Soc. Rev.* 2011, **40**, 1697.

30 S. Chen, J. Zhu, X. Wu, Q. Han and X. Wang, *Acs Nano* 2010, **4**, 2822.

31 G. Yu, L. Hu, M. Vosgueritchian, H. Wang, X. Xie, J. R. McDonough, X. Cui, Y. Cui and Z. Bao, *Nano Lett.* 2011, **11**, 2905.

32 H. Wang, H. S. Casalongue, Y. Liang and H. Dai, *J. Am. Chem. Soc.* 2010, **132**, 7472.

33 X. Cao, Y. Shi, W. Shi, G. Lu, X. Huang, Q. Yan, Q. Zhang and H. Zhang, *Small* 2011, **7**, 3163.

34 X.-C. Dong, H. Xu, X.-W. Wang, Y.-X. Huang, M. B. Chan-Park, H. Zhang, L.-H. Wang, W. Huang and P. Chen, *Acs Nano* 2012, **6**, 3206.

35 Q. Qu, S. Yang and X. Feng, *Adv. Mater.* 2011, **23**, 5574.

36 J. Yan, Z. Fan, W. Sun, G. Ning, T. Wei, Q. Zhang, R. Zhang, L. Zhi and F. Wei, *Adv. Funct. Mater.* 2012, **22**, 2632.

37 L. L. Zhang and X. S. Zhao, *Chem. Soc. Rev.* 2009, **38**, 2520.

38 P.-C. Chen, G. Shen, Y. Shi, H. Chen and C. Zhou, *Acs Nano* 2010, **4**, 4403.

39 A. L. M. Reddy, M. M. Shaijumon, S. R. Gowda and P. M. Ajayan, *J. Phys. Chem. C* 2009, **114**, 658.

40 S. D. Perera, B. Patel, N. Nijem, K. Roodenko, O. Seitz, J. P. Ferraris, Y. J. Chabal and K. J. Balkus, *Adv. Energy Mater*. 2011, **1**, 936.

41 M. Segal, *Nat. Nanotechnol.* 2009, **4**, 612.

42 K. Erickson, R. Erni, Z. Lee, N. Alem, W. Gannett and A. Zettl, *Adv. Mater.* 2010, **22**, 4467.

43 G. J. d. A. Soler-Illia, M. Jobbágy, A. E. Regazzoni and M. A. Blesa, *Chem. Mater.* 1999, **11**, 3140.

TOC

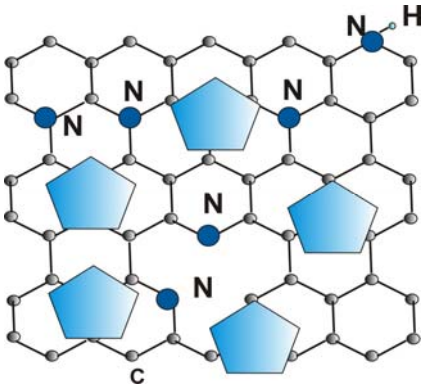

Highly nitrogen-doped graphene (N-graphene) based layered, quasi-two dimensional nanohybrids with ultrathin nanosheet nanocrystals has high performance in supercapacitor electrodes.